Hypersonic Navier-Stokes Comparisons to Orbiter Flight Data

Graham V. Candler*

Aerospace Engineering and Mechanics, University of Minnesota, Minneapolis, MN

Charles H. Campbell[†]

NASA Johnson Space Center, Houston, TX

During the STS-119 flight of Space Shuttle Discovery, two sets of surface temperature measurements were made. Under the HYTHIRM program[3] quantitative thermal images of the windward side of the Orbiter with a were taken. In addition, the Boundary Layer Transition Flight Experiment[4] made thermocouple measurements at discrete locations on the Orbiter wind side. Most of these measurements were made downstream of a surface protuberance designed to trip the boundary layer to turbulent flow. In this paper, we use the US3D computational fluid dynamics code to simulate the Orbiter flow field at conditions corresponding to the STS-119 re-entry. We employ a standard two-temperature, five-species finite-rate model for high-temperature air, and the surface catalysis model of Stewart.[1] This work is similar to the analysis of Wood et al.[2] except that we use a different approach for modeling turbulent flow. We use the one-equation Spalart-Allmaras turbulence model[8] with compressibility corrections[9] and an approach for tripping the boundary layer at discrete locations. In general, the comparison between the simulations and flight data is remarkably good. ADD DETAILS...

I. Introduction

NASA has conducted two recent experiments to measure the surface temperature of the Space Shuttle Orbiter during re-entry. In the Boundary Layer Transition Flight Experiment, a protuberance of approximately four inches in length and one-quarter inch in height was mounted on the Orbiter's port wing. Thermocouples under the tile's reaction cured glass coating were used to make measurements in the wake of the protuberance during missions STS-119 and STS-128. These data represent an important opportunity to quantitatively assess the accuracy of computational aerothermodynamics methods for an actual re-entry flight system. A recent paper describes the BLT Flight Experiment in much greater detail.[75]

Futhermore, the Hypersonic Thermodynamic Infrared Measurements (HYTHIRM) flight experiment obtained infrared images of the Orbiter windward side during three re-entries (missions STS-119, -125 and -128). These images have been converted to quantitative surface temperatures, and represent another important dataset for code assessment. Horvath *et al.*[3] discuss the full experimental campaign and companion papers present the image analysis performed on the data.[67] These data are particularly valuable because they provide detailed full-surface imagery of the Shuttle Orbiter over a wide range of flight conditions. The

---

*Professor and Fellow AIAA

[†]Aerospace Engineer, Applied Aeroscience and CFD Branch, AIAA Senior Member

American Institute of Aeronautics and Astronautics

images at high altitude show laminar flow, as well as laminar flow tripped to turbulent flow by the Flight Experiment protuberance. During STS-119 the boundary layer was tripped by an unknown roughness element, and the HYTHIRM data show this phenomenon very clearly.

The purpose of the present study is to simulate the Shuttle Orbiter re-entry and compare with the BLT Flight Experiment and HYTHIRM data. It should be stressed that these comparisons are preliminary and are subject to change and refinement. This study is similar to that of Wood et al.,[2] in which NASA codes and turbulence modeling approaches are used to simulate the Orbiter re-entry and compare to these two datasets. We use the Univesity of Minnesota US3D code to simulate the same flight conditions as Wood et al. using a different computational grid and an alternative turbulence modeling approach. The present simulations use the one-equation Reynolds-averaged Navier-Stokes Spalart-Allmaras model with a compressibility correction. To model the effect of the boundary layer protuberance and the inadvertant trip during STS-119, we use a trip model that causes the simulation to become turbulent at discrete locations. We also compute the full Orbiter geometry for three HYTHIRM cases to make direct comparisons with the infrared imagery data.

II.   Grid Generation

A new grid for the Shuttle Orbiter was generated using the GridPro grid generation software.[7] The grid was designed to resolve the windward side of the Orbiter, while providing a supersonic outflow condition. This was achieved by wrapping the grid around the fuselage and wing leading edge, so that the flow would expand to supersonic conditions before leaving the grid domain. The outer boundary of the grid was defined by a smooth surface that approximates the bow shock envelope at the lowest Mach number condition.

As in the work of Wood et al.[2] the aft end of the vehicle was simplified: the elevons are not deflected, the elevon gaps are not gridded, and the body flap is not included. Furthermore, the OML is assumed to be smooth so that any geometry variations less than a few inches in size are ignored. The flight experiment protuberance geometry is not modeled. The resulting grid for the half Orbiter has 206,400 elements on the surface, with 191 wall-normal elements, resulting in a total of nearly 40 million hexahedral elements. For the cases in which the full vehicle was computed, this grid was mirrored across the symmetry plane to obtain a grid of about 80 million elements.

Each case was run to steady-state on the baseline grid, and then the grid was shock tailored to align the grid with the bow shock. In this process, the solution along each wall-normal line of grid elements is used to find the location of the bow shock. The grid is then moved so that the shock is located at a given wall-normal grid index, and the grid points between the surface and the shock are redistributed; this redistribution is chosen so that the first grid point is located at a y^+ value of one, and a geometric grid stretching is used. In separated or low-density flow regions where the value of y^+ is large, a minimum first-point spacing is used. Several smoothing passes are then performed to improve the overall grid quality. The solution was then re-converged to a steady-state on this grid.

Figure II shows several snapshots of the grid, including the initial and final outer boundaries for Case 1, and examples of the grid resolution on the Orbiter surface. Note the smoothly-varying grid spacing and the resolution of the surface.

III.   Physical Models

The Orbiter flow fields were simulated with a standard approach: the five-species (N_2, O_2, NO, N, O) finite-rate chemical kinetics model of Park[11] with a two-temperature internal energy model was used. The effect of vibration-dissociation coupling was modeled with the $\sqrt{TT_v}$ model.[10] Standard Millikan and White V-T relaxation times were used, with corrections for some interactions from Park.[11]

The surface boundary condition was assumed to be radiative equilibrium with a partially catalytic surface based on the RCG model of Stewart.[1] The temperature-dependent catalytic efficiencies were taken from that work, and it was assumed that the surface was non-catalytic to NO molecules. The surface emissivity is

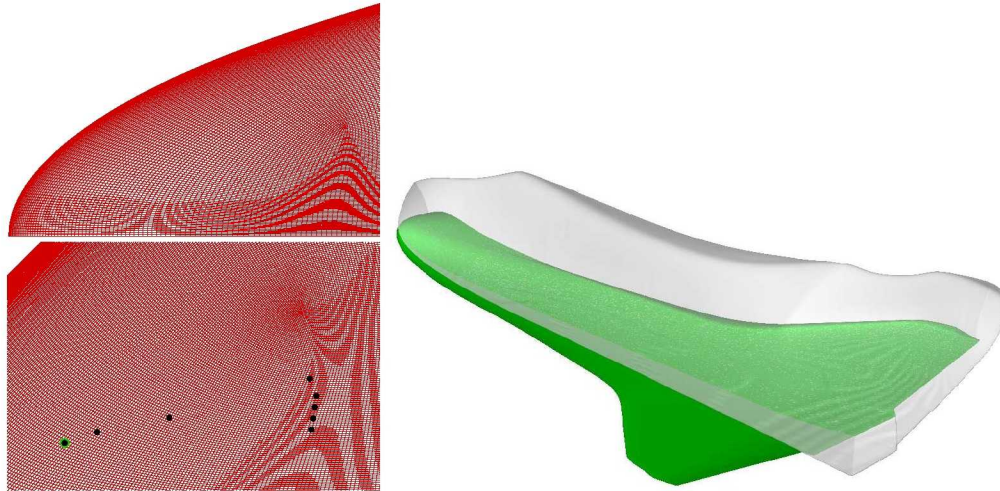American Institute of Aeronautics and Astronautics

Figure 1. Several images of the surface grid and shock-adapted outer envelop of grid for the half-Orbiter.

taken to be 0.85.

A key aspect of the present work involves the modeling of turbulent flow and how to trip the laminar boundary layer to turbulence. We use the Spalart-Allmaras one-equation RANS model[8] with the Catris-Aupoix compressibility correction.[9] The default model constants were used. The only other adjustment to the standard model involves a change to the damping function f_{v1} suggested by Sagaut et al.[12] to improve the numerical stability of the model. Details of the Spalart-Allmaras model and relevant variations to the model are available at the NASA Turbulence Modeling Resource website.[13]

The Spalart-Allmaras model is designed to preserve laminar flow until the boundary layer is tripped at a given location. The default trip model assumes that the incoming laminar boundary layer is at a high enough local Reynolds number. Then, if a small eddy viscosity source term is added near the given transition location, the eddy viscosity will grow and the boundary layer will become turbulent. In previous studies of hypersonic inlets, we found that if the boundary layer is agressively tripped with discrete trip elements, this type of trip model may not cause the boundary layer to become turbulent downstream of the trip. Instead, we impose a source term on the eddy viscosity in a Gaussian region around the trip, whose volume scales with the dimensions of the trip.

$$f_{t1} = C_t \exp\left(-2(d/h_t - 1)^2 - 2(\ell_t/d_t)^2\right)$$

where d is the distance from the wall and ℓ_t is the distance from the trip. The dimensions of the trip are h_t, its height, and d_t, its diameter. Thus, this trip term provides a source of eddy viscosity in a Gaussian volume centered at the trip, at a distance h_t from the surface. The strength of the source term can be adjusted by the coefficient, C_t. Comparisons with heat flux data taken in the CUBRC LENS-I facility at Mach 10 indicate that a value of $C_t = 0.1$ is appropriate. This model is admittedly *ad hoc* and remains to be more fully validated.

IV.   CFD Method

We use a well-developed parallel implicit CFD method, US3D,[14] to simulate a series of flows for comparison with the theory outlined above. The method uses a second-order accurate low-dissipation form of Steger-Warming flux vector splitting, and the data-parallel line-relaxation approach is used to accelerate
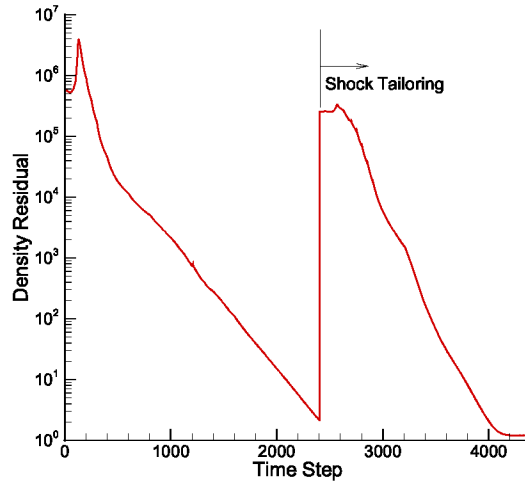
American Institute of Aeronautics and Astronautics

Figure 2. Typical convergence history for a laminar case; grid tailoring is performed once after 2400 time steps.

convergence to steady-state.[7]

The simulations were performed on a cluster of quad-core 2.3 GHz AMD Barcelona processors. The half Orbiter cases were run on 432 cores, and required 7.3 hours per 2000 time steps; the full vehicle cases were run on 864 cores in 10.0 hours per 2000 time steps. A typical convergence plot is shown in Fig. IV; seven orders of magnitude reduction in the density residual is achieved after about 2000 time steps with a maximum CFL of 4000. In this figure, the grid is shock-adapted after 2400 time steps.

V.   Comparison to STS-119 Thermocouple Data

During the STS-119 re-entry, the Shuttle Orbiter was instrumented with thermocouples to support the Boundary Layer Transition Flight Experiment. Figure IV shows the location of the thermocouples on the Orbiter planform. In these images, the flight test protuberace is located at the position of thermocouple (TC) #9. The numbering scheme used here is consistent with that used by Anderson *et al.*[4] for the first 8 thermocouples; their "Protuberance" TC is TC#9 here, and the remaining thermocouples are the usual flight instrumentation designated with a cumbersome 9 digit code. Wood *et al.*[2] use these codes and a different TC numbering scheme.

The flight TC data were obtained from Ref.;[4] the measurements were increased by 20 °F to account for the drop in temperature between the outer mold line surface and the thermocouple location.[2]

Nine flight conditions were run based on the best estimated trajectory; these are tabulated in Table 1, and are the same cases simulated by Wood *et al.*[2] Each case was run laminar, fully turbulent, and with a discrete boundary layer trip located at the flight experiment protuberance. These cases were run on one half of the Orbiter and a zero yaw angle was assumed. In addition, full Orbiter cases were run at the $t = 1197\,\text{sec}$ condition and at the $t = 1196\,\text{sec}$ condition corresponding to the HYTHIRM measurement trajectory point.

First consider the laminar heating levels early in the re-entry. As shown in Fig. 4, the CFD and flight data are generally in excellent agreement with one another. At most TC locations, the CFD over-plots the data prior to transition. Exceptions include TC#2 which is in the wake of the flight experiment protuberance, and TC#9 which is located on the protuberance itself and is not resolved by the simulation. TC#10, located near the wing leading edge, measured below the CFD early in the trajectory, but then comes into close
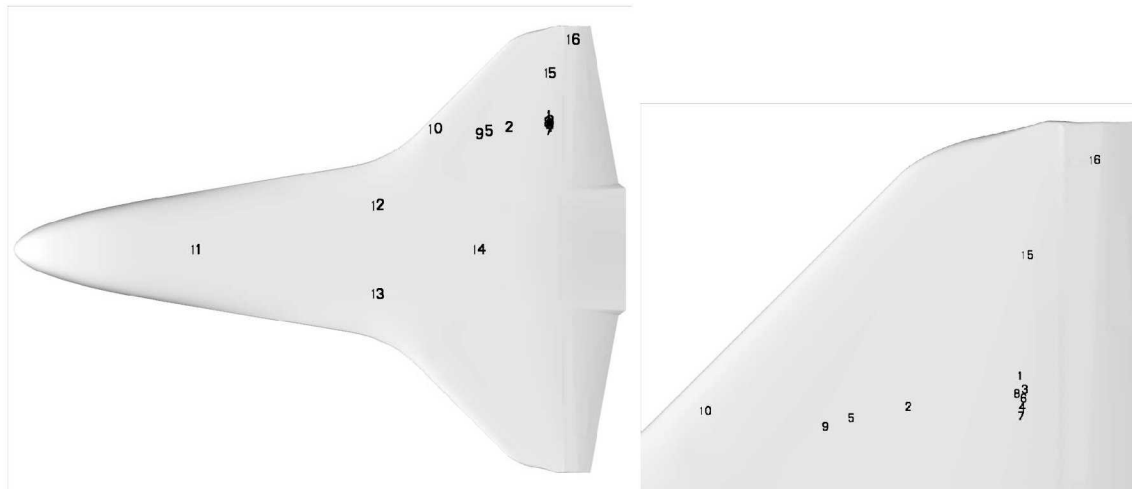
American Institute of Aeronautics and Astronautics

Figure 3. Numbering system and thermocouple locations on the windward side of the Shuttle Orbiter.

agreement prior to transition. Also, TC#15 (outboard on the port wing) is somewhat under-predicted by the CFD under laminar flow.

According to the flight data, transition on the flight experiment protuberance occurs at about 1000 seconds after entry interface. This is shown by the sudden increase in surface temperatures at the thermocouple locations in the wake of the protuberance. Thermocouples 1, 2, 3, 5, 6, and 8 show a sudden increase at this time; the TCs at the more inboard locations, 4 and 7, have a delay of about 200 seconds before becoming fully turbulent. Thus, the inboard edge of the turbulent wedge is located approximately between TC#6 and 4. As the Mach number decreases during entry, the spreading of the turbulent wedge increases and the TCs 4 and 7 experience turbulent flow.

The CFD generally predicts the fully turbulent heating levels very well. The BLT Flight Experiment data are over-plotted by the CFD for TCs 1–8. TC#5 shows some jitter, which falls around the CFD prediction; the variation in the measurements is presumably due to the location of this TC in the wake of the protuberance. As expected, the flight data on TC#9 are higher than the smooth OML simulations.

The CFD runs with a discrete trip (green lines in Fig. 4) are essentially the same as the fully turbulent simulations for TCs 1–8. That is because the trip model produces a large turbulent wedge that rapidly expands downstream and produces fully turbulent flow over all flight experiment TCs. Thus, the CFD does not properly capture the slow growth of the turbulent wedge that produces the delay in turbulent heating levels at TCs 4 and 7. Figure VI shows the predicted surface temperature at the $t = xxx$sec time to illustrate the effect of the trip model downstream of the protuberance. Note that in this figure the surface temperature is lower on the inboard portion of the turbulent wedge, which is consistent with the thermocouple data. RUN A CASE LIKE THIS WITH A WEAKER TRIP FORCING FUNCTION.

Now consider the predictions for the thermocouples on the remainder of the Orbiter (TCs 10–16). In the half-orbiter simulations, the trip model only affects the flow downstream of the protuberance, and therefore there is no difference between the laminar and tripped turbulent predictions for these TCs. In the full-orbiter simulations, an additional discrete boundary layer trip was added to mimic the turbulent flow observed during the HYTHIRM experiment for STS-119. This trip was located near the corner of the nose landing gear door, and was assumed to have the same magnitude as the flight experiment protuberance trip. As will be illustrated below, the turbulent wedge emanating from the nose gear trip covers some of the TCs with turbulent flow, while leaving the outboard TCs unaffected.

In general, the simulations are in good agreement with TCs 10–16. The turbulent levels agree very

American Institute of Aeronautics and Astronautics

well once the flow has become fully turbulent. Moreover, the full Orbiter simulations agree very well at all locations except for TC#16 (at the most outboard location on the port wing).

It should be noted that for the radiative equilibrium surface condition used here, the heat transfer rate scales with the surface temperature to the fourth power. Thus, small differences in surface temperature result in larger discrepancies in the heat flux.

In the present simulations, we assumed a surface emmissivity of 0.85, whereas Wood *et al.* use $\epsilon = 0.89$. We reran one fully turbulent case at the $t = 1031$ sec condition to assess the sensitivity of the surface temperature to this modeling difference. Figure VI plots the difference in surface temperature; note that the maximum temperature difference is 50 °F and that for most of the data taking region the difference is less than 25 °F. (The lower value of emmissivity results in larger surface temperature.)

Table 1. Simulation conditions.

Mission	t (sec)	Mach	V_∞ (m/s)	α (deg)	β (deg)	T_∞ (K)	ρ_∞ (kg/m^3)
	834	19.36	5956	39.20	0.06	235.5	1.526×10^{-4}
	923	17.04	5386	42.12	0.48	248.5	2.283×10^{-4}
	1031	13.52	4398	38.98	-0.03	263.3	5.075×10^{-4}
	1051	12.88	4200	39.32	0.14	264.6	5.484×10^{-4}
STS-119	1125	10.51	3466	39.18	0.17	270.7	8.184×10^{-4}
	1172	9.10	3002	38.31	0.24	270.7	1.104×10^{-3}
	1197	8.41	2772	37.60	0.12	270.7	1.244×10^{-3}
	1233	7.51	2469	35.23	0.02	268.9	1.641×10^{-3}
	1319	5.77	1831	27.97	0.03	250.7	4.014×10^{-3}
STS-119	1196	8.43	2781	37.65	0.20	270.7	1.234×10^{-3}
STS-125	991	14.33	4642	41.69	-0.04	260.5	4.364×10^{-4}
STS-128	1005	14.73	4760	41.97	-0.01	259.2	3.836×10^{-4}

VI.   Results

VII.   Comparison to HYTHIRM IR Imagery Data

Three full-Orbiter cases were run to compare with the HYTHIRM measurements discussed by Horvath *et al.*[3] The conditions are tabulated in Table 1. For the STS-119 mission, a discrete boundary layer trip was added at the approximate location of the corner of the nose landing gear door, as well as at the BLT Flight Experiment location. For STS-125, the flow was taken to be fully laminar because the measurements were made early in the trajectory and there is no evidence of early transition. For STS-128, a boundary layer trip was added at the location of the flight experiment protuberance.

Figure VII is a contour plot of the predicted surface temperature for the STS-119 mission.

Figure XX is a contour plot of the predicted surface temperature for the STS-125 mission. [CASE IS RUNNING: will be updated when complete.

Figure XX is a contour plot of the predicted surface temperature for the STS-128 mission. [CASE IS RUNNING: will be updated when complete.

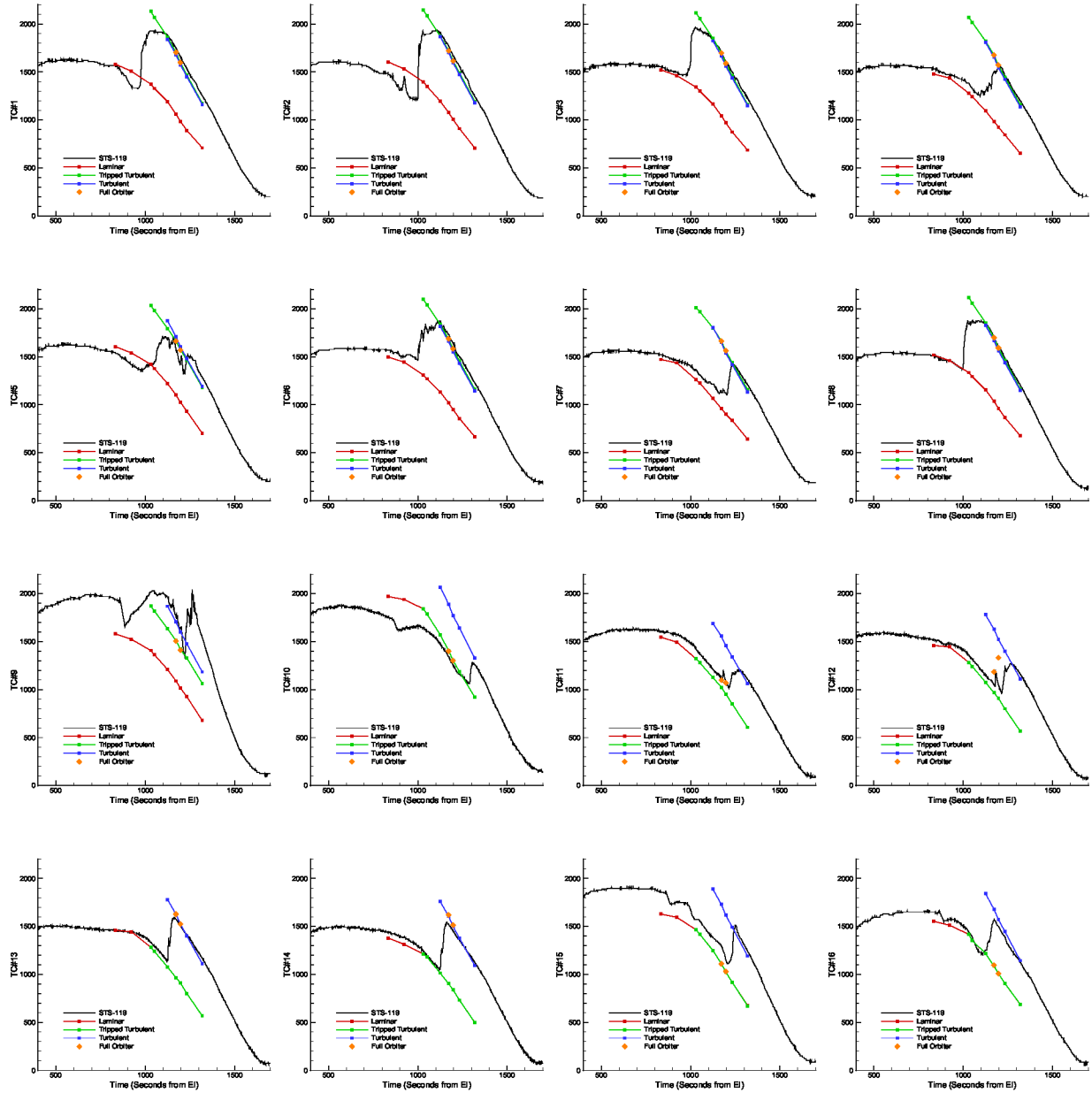NOTE: I would like to show images from the Horvath paper if possible.

American Institute of Aeronautics and Astronautics

Figure 4. Comparison to thermocouple data from STS-119 (surface temperature in °F).

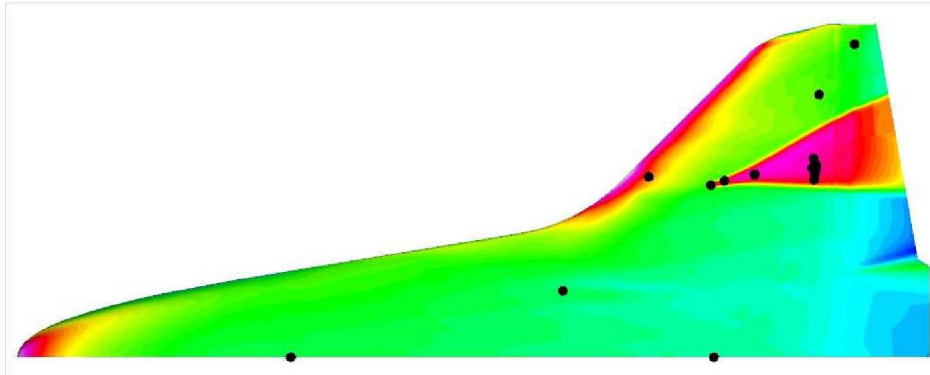American Institute of Aeronautics and Astronautics

Figure 5. Computed surface temperature at $t = 1125\,\text{sec}$ for STS-119 mission, showing the effect of the boundary layer trip.
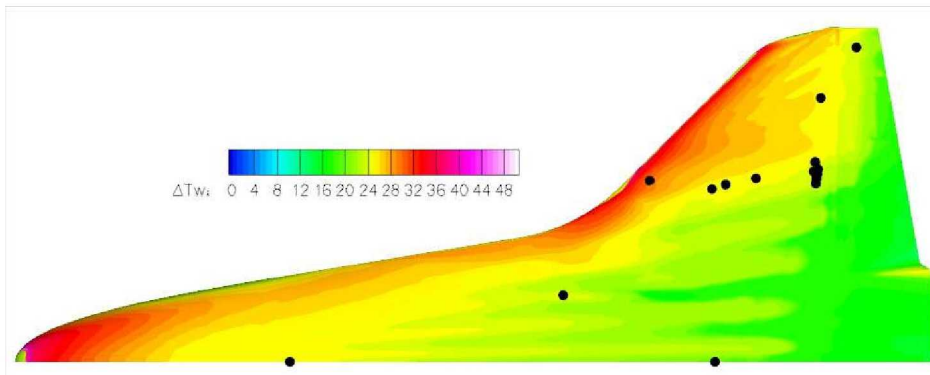

Figure 6. Computed change in surface temperature (°F) at $t = 1031\,\text{sec}$ for STS-119 mission; laminar flow.

VIII. Conclusion

Acknowledgments

References

[1]Stewart D.A. "Surface Catalysis and Characterization of Proposed Candidate TPS for Access-to-Space Vehicles," NASA TM-112206 1997.

[2]Wood, W.A., W.L. Kleb, C.Y. Tang, G.E. Palmer, A.J. Hyatt, A.J. Wise and P.L. McCloud, "Comparison of CFD Predictions with Shuttle Global Flight Thermal Imagery and Discrete Surface Measurements, AIAA-2010-0454, Jan. 2010.

[3]Horvath, T.J., D.M. Tomek, K.T. Berger, S.C. Splinter, J.N. Zalameda, P.W. Krasa, R.J. Schwartz, D.M. Gibson and A. Tietjen, "The HYTHIRM Project: Flight Thermography of the Space Shuttle During Hypersonic Re-Entry," AIAA-2010-0241, Jan. 2010.

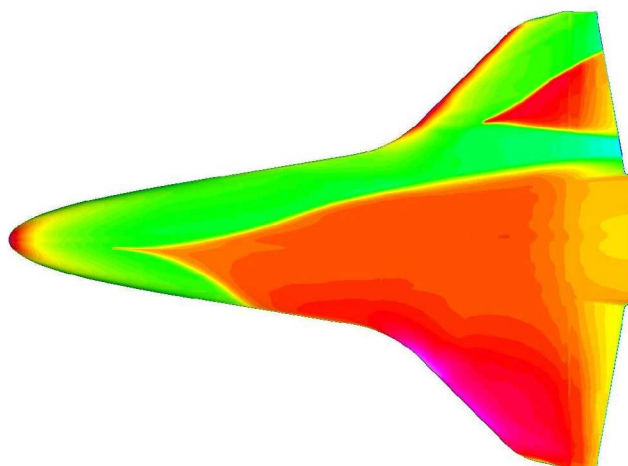[4]Anderson, B., C.H. Campbell, L.A. Saucedo and G.R. Kinder, "BLT Flight Experiment Overview and In-Situ Measure-

American Institute of Aeronautics and Astronautics

Figure 7. Computed surface temperature for the STS-119 mission at 1196sec **after entry interface, corresponding to the HYTHIRM NIR imagery.**[3]

ments," AIAA-2010-0240, Jan. 2010.

[5]Spanos, T., G.R. Kinder, C.H. Campbell, J. Andress, "Design and Implementation of the Boundary Layer Transition Flight Experiment on Space Shuttle Discovery," AIAA-2010-0242, Jan. 2010.

[6]Gibson, D., T. Spisz, J. Taylor, J.N. Zalameda, T.J. Horvath, D.M. Tomek, A. Tietjen, S. Tack and B. Bush, "HYTHIRM Radiance Modeling and Image Analyses in Support of STS-119 and STS-125 Space ShuttleHypersonic Re- Entries," AIAA-2010-0244, Jan. 2010.

[7]Zalameda, J.N., T.J. Horvath, D.M. Tomek, A. Tietjen, D. Gibson and D. Merce, "Calibration of a Near Infrared Imaging System for Thermographic Imaging of the Space Shuttle during Hypersonic Re-Entry," AIAA-2010-0245, Jan. 2010.

[8]Spalart, P.R., and Allmaras, S.R., "A One-Equation Turbulence Model for Aerodynamic Flows," AIAA Paper 92-0439, Jan. 1992.

[9]Catris, S., and B. Aupoix, "Density Corrections for Turbulence Models," *Aerospace Science and Technology,* Vol. 4, 2000, pp. 1-11.

[10]Park, C., "Assessment of Two-Temperature Kinetic Model for Ionizing Air," *AIAA Paper No. 87-1574,* June 1987.

[11]Park, C., *Nonequilibrium Hypersonic Aerothermodynamics,* Wiley, 1990.

[12]Sagaut, P., S. Deck and M. Terracol, *Multiscale and Multiresolution Approaches in Turbulence,* Imperial College Press, p. 257, 2006.

[13]Rumsey, C., http://turbmodels.larc.nasa.gov/spalart.html

[14]Nompelis, I., Drayna, T. W. and Candler, G. V., (2005), A Parallel Unstructured Implicit Solver for Reacting Flow Simulation," AIAA 2005-4867, June 2005.

American Institute of Aeronautics and Astronautics